

VIP Very Important Paper

Special Collection

Mechanistic Understanding of Oxygen Electrodes in Rechargeable Multivalent Metal–Oxygen Batteries

Zhuojian Liang^[a] and Yi-Chun Lu^{*[a]}

Rechargeable multivalent metal–O₂ batteries (Mg–O₂, Zn–O₂ and Al–O₂ etc.) are promising next-generation battery technologies for electric automobiles and large-scale energy storage owing to their high energy density, low cost, and sustainability. To realize the full potentials of these systems, an in-depth mechanistic understanding of the underlying chemistries is crucial for rational development. However, compared with the intensively studied Li–O₂ batteries, reaction mechanisms of

multivalent metal–O₂ batteries are much less understood. Here, we discuss the current status of mechanistic understanding of oxygen reduction and evolution reactions in rechargeable multivalent metal–O₂ batteries. We discuss the key open questions and future research directions of multivalent metal–O₂ batteries using examples and experiences from Li–O₂ batteries, which could guide and inspire the development of multivalent metal–O₂ batteries.

1. Introduction

High-energy-density, low-cost, and sustainable rechargeable batteries are critical foundations for wide market penetration of electric vehicles and stationary energy storage. Although current Li-ion batteries have achieved great success in these applications, they are limited by their energy density (200 Wh/kg).^[1] The research community has been actively exploring new chemistries to advance towards high-energy batteries. Among the diverse systems, rechargeable metal–O₂ batteries are promising in meeting the energy requirements.

Metal–O₂ batteries combine a metal anode and a porous cathode in which O₂ acts as the active material to provide superior energy density compared to Li-ion batteries. Theoretically, metal–O₂ batteries promise specific energies up to 5,220 Wh/kg (Li–O₂ batteries based on Li₂O) and energy densities up to 17,027 Wh/L (Al–O₂ batteries based on Al₂O₃). Practically, metal–O₂ batteries could achieve 3–5-fold higher specific energy than current Li-ion batteries.^[1] In addition, without expensive elements such as Co in their active materials, the material cost of these batteries can be drastically lower than state-of-the-art Li-ion batteries. The stability of some multivalent metals in air, e.g. Al, Mg, Fe and Zn, could substantially improve the safety of rechargeable batteries over the Li/Na/K metal batteries. Contrary to the reactivity of alkali metal oxides (e.g. Li₂O₂, Na₂O₂) with air components (CO₂ and H₂O), which requires the use of pure O₂ or air purification system, the stability of these multivalent metals oxides in the

air could allow the direct use of atmospheric air, which further reduces the cost and simplifies the battery structure.

The development of rechargeable multivalent metal–O₂ batteries is still in its infancy. Most of the multivalent metal–O₂ batteries are limited by poor cycle life (the best being 320 cycles of Zn–O₂ batteries,^[2] while less than 5 cycles in some other systems) and high energy loss. Improving the cycling stability and energy efficiency is strongly limited by the lack of understanding of the reaction mechanisms of the oxygen reduction reaction (ORR) and oxygen evolution reaction (OER). Resolving mechanistic open questions in reaction mechanism and degradation mechanism is one of the most crucial tasks in developing rechargeable multivalent metal–O₂ batteries.

Here, we first review the current status of mechanistic studies on oxygen electrodes in rechargeable multivalent metal–O₂ batteries. We then discuss future research directions of multivalent metal–O₂ batteries using examples and experiences learning from Li–O₂ batteries, which could guide and inspire the development of multivalent metal–O₂ batteries. Key open questions in the ORR and OER mechanism are identified.

2. Current Status of Mechanistic Understanding

2.1. Zn–O₂ Batteries

Most studies on Zn–O₂ batteries exploit alkaline aqueous electrolytes, which have been well studied for Zn-based batteries, yielding ZnO as the discharge product, which precipitates on the anode. However, Zn anode [$E^0 = -0.76$ V vs. standard hydrogen electrode (SHE), and < -1.2 V vs. SHE in strongly alkaline solutions] shows low coulombic efficiency (CE, below 93% and sometimes even $< 50\%$) in alkaline electrolyte due to H₂ evolution reaction (HER) and decay of Zn anode (Zn dendrite and ‘dead ZnO’),^[3] limiting the cycle life of alkaline Zn–O₂ batteries to < 100 cycles.^[4] In addition, alkaline electro-

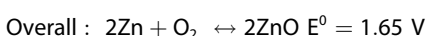
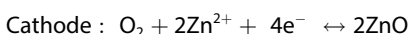
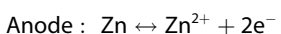
[a] Dr. Z. Liang, Prof. Y.-C. Lu

Electrochemical Energy and Interfaces Laboratory,
Department of Mechanical and Automation Engineering
The Chinese University of Hong Kong
Shatin, NT, Hong Kong SAR, China
E-mail: yichunlu@mae.cuhk.edu.hk

 An invited contribution to a joint Special Collection between ChemElectroChem and Batteries & Supercaps dedicated to research Beyond Lithium-Ion Batteries

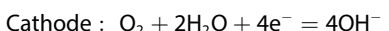
lytes react with CO_2 from the air to yield K_2CO_3 that passivates the cathode. Recent research effort has achieved Zn anode CE over 95% in three types of electrolytes,^[3b] namely ionic liquid analogues (including water-in-salt electrolytes and deep-eutectic electrolytes),^[3a,5] neutral or mildly acidic dilute aqueous electrolytes,^[6] and organic electrolytes.^[7]

Zn–O₂ batteries with water-in-salt electrolytes {1 m zinc bis (trifluoromethanesulfonyl)imide $[\text{Zn}(\text{TFSI})_2] + 20 \text{ m LiTFSI}$, where m is molality, mol/kg} were reported to yield ZnO as the discharge product.^[3a,5a]



The formation and removal of ZnO on the cathode have been confirmed by X-ray diffraction (XRD), Raman spectra, energy-dispersive X-ray spectroscopy (EDX) and scanning electron microscope (SEM) (Figure 1b, d, e and f).^[3a,5a] The ZnO crystals exhibit well-defined hexagonal prism morphology (Figure 1, d and g).^[3a] Up to 200 cycles was demonstrated (Figure 1a).^[3a,5a]

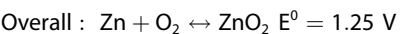
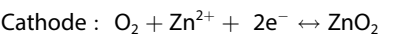
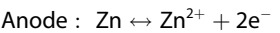
Recently, a new neutral dilute aqueous electrolyte of 1 m zinc trifluoromethanesulfonate $[\text{Zn}(\text{OTf})_2]$ in H₂O was proposed as a Zn–O₂ electrolyte that enables ZnO₂ generation in discharge.^[2] Conventionally, Zn–O₂ batteries with neutral dilute aqueous electrolyte generates OH[−] during ORR:



which then reacts with ZnSO₄ to trigger precipitation of a low-specific-energy discharge product, e.g. $\text{ZnSO}_4[\text{Zn}(\text{OH})_2]_3 \cdot 0.5\text{H}_2\text{O}$,^[8] resulting in lower energy density. In the new electrolyte, according to multiscale simulations,^[2] the new chemistry was enabled by the hydrophobicity of the OTf[−] anions, which results in a water-poor and Zn²⁺-rich inner Helmholtz layer in the cathode, in which a Zn²⁺-assisted 2e[−]/O₂ ORR pathway without water participation is favored over the conventional H₂O-involving 4e[−]/O₂ ORR pathway:



Zhuojian Liang received his Ph.D. at the Chinese University of Hong Kong (CUHK) in 2018. Since joining Prof. Yi-Chun Lu's group at CUHK in 2013, he has been actively developing mechanistic understanding of Li–O₂ batteries using operando techniques and exploring novel solutions to the instabilities. His current research focuses on developing new electrolytes and novel battery configurations for metal–O₂ batteries.



The reversible formation and removal of fiber-shaped ZnO₂ were comprehensively supported by SEM (Figure 1h), XRD (Figure 1h), EDX, Raman and XPS. Operando pressure measurement (Figure 1i) confirms ~2 e[−]/O₂ ratios in both ORR and OER. The stable cycling voltage profiles (Figure 1j) indicate high reversibility of this new chemistry. Up to 320 cycles were demonstrated at 1.0 mA cm^{−2}.^[2]

With the primary discharge product identified as ZnO/ZnO₂, more characterization is needed to quantify the yield of ZnO/ZnO₂ and probe parasitic reactions that degrade the cathode. For instance, Wang *et al.*, Chen *et al.* and Sun *et al.* observed that the discharge voltage of Zn–O₂ cells gradually decayed upon cycling (Figure 1a and c), which was attributed to catalyst aggregation and loss of active area on the cathode due to passivation by a solid layer of by-products, as supported by SEM.^[3a,5a] Besides, cathode degradation by side reactions is also possible. In fact, Raman spectrum of the Zn–O₂ cathode cycled in 1 m zinc Zn(TFSI)₂+20 m LiTFSI electrolyte indicated the formation of Li₂CO₃ (Figure 1b).^[5a] This could result from reaction with CO₂ from the air, or degradation of the TFSI[−] ion on the cathode triggered by potential intermediates in the electrochemical formation and decomposition of ZnO, e.g. superoxide and singlet O₂ (¹O₂), which has been reported in Li–O₂ batteries to be associated with electrolyte degradation^[9] (discussed in detail in Section 3). In the Zn–O₂ cells cycled in ZnCl₂·2.33H₂O electrolyte, the authors reported Cl₂ gas evolution at a yield of <0.8%.^[3a] Future studies could explore suppressing Cl₂ evolution by reducing the charge potential with catalyst, as Cl₂ evolution not only irreversibly decomposes electrolyte salts but also corrodes cell components including cell case and current collectors.

Identifying the discharge intermediate(s) and quantifying their solubility are important for improving the rate capability and discharge capacity of Zn–O₂ batteries. The discharge overpotential was ~800 mV at current densities of 0.035~



Yi-Chun Lu is an Associate Professor of Mechanical and Automation Engineering at the Chinese University of Hong Kong (CUHK). She received her B.S. degree in Materials Science & Engineering from National Tsing Hua University, Taiwan in 2007 and earned her Ph.D. degree in Materials Science & Engineering from Massachusetts Institute of Technology in 2012. Prof. Lu worked as a Postdoctoral Fellow in the Department of Chemistry at the Technische Universität München, Germany in 2013 before joining CUHK. Prof. Lu's research interest centers on fundamental redox chemistry and developing functional materials for clean energy storage and conversion.

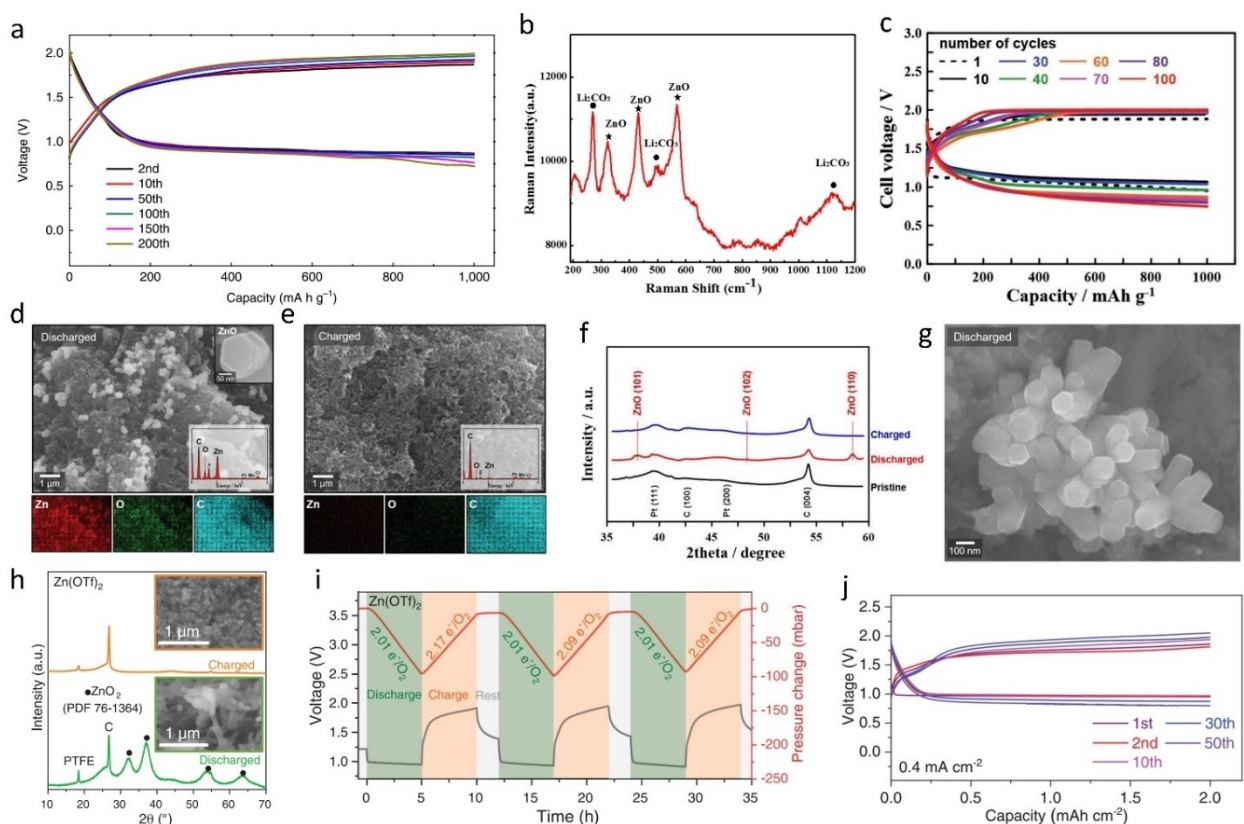


Figure 1. Mechanistic characterization of $\text{Zn}-\text{O}_2$ batteries. a) Cycling performance of the Zn/O_2 battery with $1 \text{ M} \text{Zn}(\text{TFSI})_2 + 20 \text{ M LiTFSI}$ aqueous electrolyte at a current density of 50 mA/g (areal capacity 0.7 mAh/cm^2). b) Raman spectrum of the cycled cathode at the discharge state of the Zn/O_2 cell. Reproduced from Ref. [5a] with permission. Copyright 2018, Springer Nature. c) Cycling performance of the $\text{Zn}-\text{air}$ cell with $\text{ZnCl}_2 \cdot 2.33\text{H}_2\text{O}$ electrolyte at a current density of 500 mA/g (areal capacity 0.5 mAh/cm^2). SEM images, EDX analysis, and elemental mapping of the Pt/C cathodes at d) the discharge state and e) the charge state. f) XRD patterns of Pt/C cathodes recovered from the $\text{Zn}-\text{air}$ cell. g) SEM images of the discharged Pt/C cathode. Reproduced from Ref. [3a] with permission. Copyright 2019, Wiley-VCH. h) XRD patterns and SEM images of air cathodes obtained after discharge and recharge in $\text{Zn}(\text{OTf})_2$ electrolyte. i) Pressure change of $\text{Zn}-\text{O}_2$ cells during galvanostatic cycling at 0.4 mA/cm^2 . j) Galvanostatic cycling at a fixed capacity of 2.0 mAh/cm^2 and a current density of 0.4 mA/cm^2 . Reproduced from Ref. [2] with permission. Copyright 2021, American Association for the Advancement of Science.

4.0 mA/cm^2 in these initial studies.^[2–3,5a] This could be limited by multiple factors including the solubility of intermediate(s) and/or diffusivity of O_2 . The solubility of ORR intermediates, which depends on electrolyte properties, governs the competition between the surface-discharge-pathway and the solution-discharge-pathway. In the solution pathway, intermediates dissolve into the electrolyte after their formation on the cathode and diffuse to the surface of existing discharge product for further reactions, which frees the cathode surface from blocking by discharge products, leading to higher discharge current densities and larger discharge capacity. The three-dimensional growth of ZnO crystal indicates some solubility of the intermediate(s), yet the small dimension of a few hundreds of nanometers suggests that the solubility is low. Improving the solubility of intermediate(s) by the use of solvent or additives with higher donor and/or acceptor numbers,^[10] e.g. crown ethers^[11] and borates,^[12] could improve the discharge performance. Under large current densities, the diffusion rate of O_2 from the electrolyte/gas interface to the cathode surface could be limiting and contributes to overpotential. The use of solvents and additives that display high O_2 solubilities and

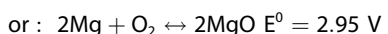
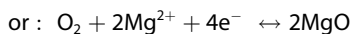
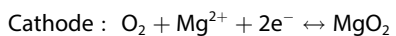
diffusivities, e.g. ionic liquids^[13] and perfluorinated carbon liquids,^[14] are worth exploring.

2.2. Mg–O₂ Batteries

Aqueous Mg–O₂ batteries are primary batteries^[15] due to the irreversibility of aqueous Mg anode, which reacts at a substantially lower potential than HER ($E^\circ = -2.37 \text{ V}$ vs. SHE). To enable reversible Mg–O₂ batteries, electrolytes that allow reversible plating and stripping of Mg metal must be used. High Mg anode CE of 98%~100% are reported in multiple types of electrolytes, including simple-salt-based electrolytes,^[16] Mg–Cl-complex-based electrolytes^[17] and boron-based electrolytes,^[18] whose application in rechargeable Mg–O₂ batteries could be explored.

Theoretical studies have shown that both MgO_2 and MgO are possible discharge products at ambient temperature and pressure:^[19]





Investigations on ORR mechanism in simple-salt-based electrolyte agree with these theoretical studies. In the electrolyte of $\text{Mg}(\text{ClO}_4)_2$ in dimethyl sulfoxide (DMSO), Reinsberg *et al.* studied the influence of electrode material on ORR and OER mechanisms using rotating ring-disc electrode (RRDE) and *operando* electrochemical mass spectrometry (OEMS) (Figure 2a-c).^[20] In the cathodic scan on RRDE (Figure 2c), they found that ORR proceeded at $2\text{e}^-/\text{O}_2$ on GC, Au and Pt, which agrees with the formation of MgO_2 , and $\sim 2.4\text{e}^-/\text{O}_2$ on Ru and up to $\sim 3.8\text{e}^-/\text{O}_2$ on Rh, which suggest additional concurrent formation of MgO or by-products. They discovered an increase of collection efficiency at the ring with increasing rotation rate, which implies chemical reactions after the initial step of ORR, e.g. further reduction or precipitation of the discharge

intermediate and/or product, or other side reactions.^[20] In the anodic scan, despite the detection of strong oxidative current, neither O_2 nor parasitic gases like CO_2 were observed (Figure 2a), which indicates that the discharge product(s) could not be reversibly oxidized on Pt in DMSO. These findings were further corroborated by Fischer *et al.*,^[21] who found evidence of MgO_2 on the discharged Pt and Au cathodes with XPS (O_2^- peak in $\text{O}\ 1\text{s}$ spectra and an O:Mg ratio of 2.2) at a high yield of 96%, as well as peaks of by-products such as MgCl_2 and dimethyl sulfone (DMSO₂).

$\text{Mg}-\text{O}_2$ reaction products vary significantly between Mg–Cl-complex-based electrolytes. Vardar *et al.* identified the discharge product as a mixture of MgO_2 and MgO in the all-phenyl-complex (APC) electrolyte [$\text{PhMgCl} + \text{Al(OPh)}_3$] in tetrahydrofuran (THF).^[19a] They observed the formation and decomposition of MgO on the cathode with XRD and Raman (Figure 2d–e). Auger electron spectroscopy (AES) confirmed the presence of Mg and O in the discharge products, amounting to a $\text{MgO}_2:\text{MgO}$ molar ratio of 1:3.3 (Figure 2f). The large particle size ($\sim 200 \mu\text{m}$) observed via SEM (Figure 2g) indicates that either the discharge intermediate is highly soluble or that the discharge product is conductive, both of which are beneficial

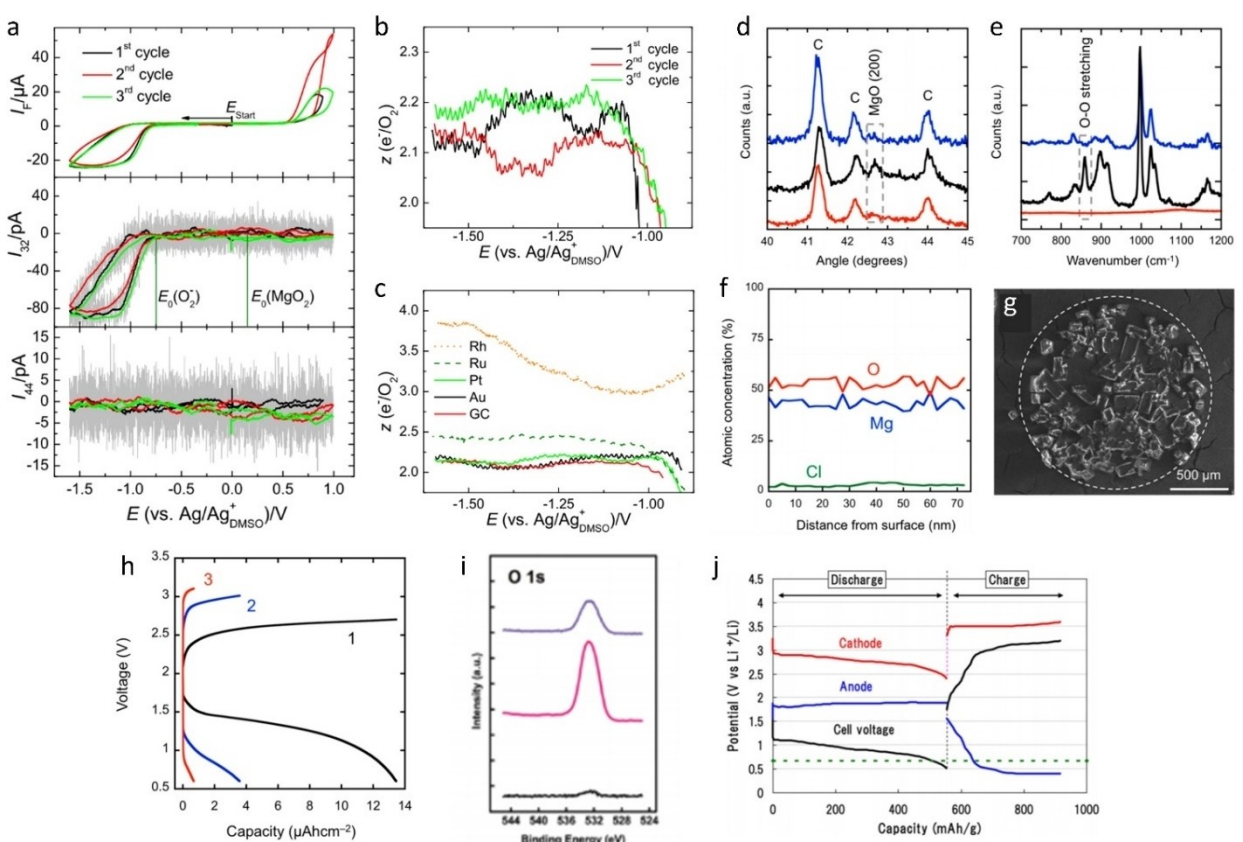


Figure 2. Mechanistic characterization of $\text{Mg}-\text{O}_2$ batteries. a) CV and OEMS results on a Pt cathode with $\text{Mg}(\text{ClO}_4)_2$ - DMSO electrolyte. The number of electrons transferred per oxygen molecule on b) Pt and c) multiple cathodes. Reproduced from Ref. [20] with permission. Copyright 2016, Elsevier. d) XRD pattern of control (red), discharged (black) and recharged (blue) carbon cathodes in APC electrolyte. e) Raman spectra collected from control (red), discharged (black), and recharged (blue) carbon cathodes. f) AES depth profile of the discharge product. g) SEM images of the discharged cathode. h) Discharge-charge cycles for a $\text{Mg}-\text{O}_2$ cell at $5 \mu\text{A}/\text{cm}^2$. Reproduced from Ref. [19a] with permission. Copyright 2015, American Chemical Society. i) O 1s XPS spectra of the as-prepared (black traces), discharged (pink traces) and fully recharged (violet traces) carbon paper cathodes in the electrolyte with dual mediators. Reproduced from Ref. [22] with permission. Copyright 2016, Royal Society of Chemistry. j) Discharge-charge profile of a $\text{Mg}-\text{O}_2$ cell in a three-electrode cell with a Li/Li^+ reference electrode. Reproduced from Ref. [23] with permission. Copyright 2014, American Chemical Society.

for realizing large discharge capacity. Both AES and SEM showed that the discharge product was only partly removed during charge, suggesting the existence of side reaction(s). On the contrary, although the identical porous carbon cathodes were used, no MgO_2 or MgO was found in Mg-Al-chloride-complex (MACC) electrolyte [$\text{MgCl}_2 + \text{AlCl}_3$ in dimethoxyethane (DME)] after discharge.^[24] Instead, XRD revealed only precipitations of MgCl_2 and $\text{Mg}(\text{ClO}_4)_2$ on the discharged cathode. The different discharge products in APC and MACC electrolyte indicate that the discharge reaction is sensitive to not only the type of the working ion (e.g. Mg-Cl complex or Mg^{2+}) but also to other existing species in the electrolyte.

The use of redox mediators has been reported in simple-salt-based electrolytes.^[22–23,25] Mediators are soluble and electrochemically active species that act as charge carriers in the electrolyte during cycling. For example, in metal- O_2 batteries, a charge mediator facilitates the oxidation of metal (su)(per)oxides into O_2 . During charge, the mediator is firstly oxidized, diffuses to the discharge products, and oxidizes them to evolve O_2 , during which the mediator is reduced back to its original state. Similarly, a discharge mediator facilitates the reduction of O_2 to (su)(per)oxides. The observed (dis)charge potential of the cell is determined by the redox potential of this (dis)charge mediator, which should be higher than the reversible potential of OER (or lower than that of ORR) to provide driving force of the chemical redox reactions. Shiga *et al.* first showed that a $\text{Mg}-\text{O}_2$ battery with $\text{Mg}(\text{ClO}_4)_2$ in DMSO electrolyte can discharge to form MgO as revealed by time-of-flight mass spectrometry (ToF-MS), however, the cell could not be recharged.^[25] They showed that the addition of I_2 into a MgO suspension could dissolve MgO to evolve O_2 , and attributed this to the oxidation of MgO by DMSO- I_2 complex. With I_2 in the electrolyte, charging voltage was reduced while O_2 was detected by gas chromatography mass spectrometry (GCMS). As a result, the cell could sustain four galvanostatic cycles. The authors further applied 2,2,6,6-Tetramethyl-1-piperidinyloxy (TEMPO) as a charge mediator with $\text{Mg}(\text{TFSI})_2$ in diethyl-methylmethoxymethylpiperidium bis(trifluoromethanesulfonyl)imide (DEMETFSI) electrolyte, in which the discharge products are yet to be identified. To prove the chemical reactivity, they showed that TEMPO⁺-containing solution could dissolve MgO to evolve O_2 . They further showed that charging with TEMPO lowered the voltage. Consistently, EDX mapping revealed a lower Mg coverage on the charged cathode and O_2 evolution was detected using GCMS. To further facilitate discharge reaction, Dong *et al.* proposed using dual redox mediators {1,4-benzoquinone (BQ) and 5,10,15,20-tetraphenyl-21H,23H-porphine cobalt(II) [Co(II)TPP]} for rechargeable $\text{Mg}-\text{O}_2$ batteries.^[22] Cycling with dual mediators reduced overpotentials for both discharge and charge. Pressure in the cell reduced during discharge and increased during charge, and X-ray photo-electron spectroscopy (XPS) of the discharged cathode revealed MgO_2 as the discharge product (Figure 2i).^[21–22] These three studies demonstrated MgO_2/MgO and O_2 as possible products of discharge and charge, respectively. However, some cycling capacity could be contributed by the mediators alone. If the charge mediator is electrochemically oxidized but fails to

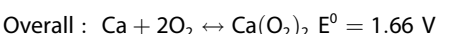
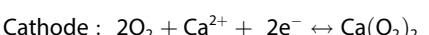
oxidize the discharge product, the charged mediator could be electrochemically reduced in the subsequent discharge (contributing capacity). Based on theoretical standard potentials, neither MgO_2 (2.94 V vs. Mg/Mg^{2+}) nor MgO (2.95 V vs. Mg/Mg^{2+}) could be oxidized by I_3^-/I_2 (around 2.0 V~2.5 V vs. Mg/Mg^{2+})^[26] or TEMPO/TEMPO⁺ (~2.8 V vs. Mg/Mg^{2+}).^[27] Future studies using quantitative techniques would help to understand the mediation mechanisms.

The low discharge voltage of the $\text{Mg}-\text{O}_2$ battery (~2.0 V, Figure 2h) significantly deviates from the reversible potentials of both MgO_2 (2.94 V vs. Mg/Mg^{2+}) and MgO (2.95 V vs. Mg/Mg^{2+}).^[19a] The oxygen electrode potential could be better revealed by using three-electrode cell, which could differentiate the overpotential contribution between anode and cathode.^[23,25] For instance, Figure 2j shows that the overpotential of the Mg anode could significantly dominate the $\text{Mg}-\text{O}_2$ cells, preventing accurate understanding of the oxygen electrode potential.

2.3. Ca- O_2 Batteries

While reversible plating and stripping of Ca metal ($E^0 = -2.87$ V vs. SHE) are challenging, recent efforts have realized facile reactions with CE up to 96% in organic electrolytes, enabling the exploration of rechargeable batteries with a Ca metal anode.^[28]

Various studies have found that ORR in the presence of Ca^{2+} yields superoxide or oxide depending on cathode materials. Reinsberg *et al.* studied ORR and OER using RRDE and OEMS.^[29] On multiple materials, i.e. GC, Pt, Ru and Rh, they found that ORR proceeded at ~1e⁻/ O_2 (Figure 3b), and yielded discharge product that could be oxidized back to O_2 at ~1e⁻/ O_2 (Figure 3a), which implies the formation of $\text{Ca}(\text{O}_2)_2$ with a high reversibility:^[29a]



The onset potentials of ORR and OER were ~−0.8 V and ~0.2 V vs. Ag/Ag^+ [~2.6 V and ~3.6 V vs. Ca/Ca^{2+} , based on $E(\text{Ag}/\text{Ag}^+) = 3.36$ V vs. Ca/Ca^{2+} they used], respectively (Figure 3a). Interestingly, the ORR onset potential is substantially higher than the reversible potential calculated from thermodynamic data, which could result from the stabilization of O_2^- by the cation.^[30] The high roundtrip overpotentials of around 1 V were attributed to the formation of contact ion-pair between Ca^{2+} and O_2^{2-} . The discharge product was fairly soluble, with ~90% dissolved in the electrolyte and only ~5% deposited on the cathode under the reported testing conditions.^[29] The remaining 5% of reduced oxygen species was decomposed, which was found to depend on the water content of the electrolyte.^[29] The ratio of dissolved superoxide could be affected by the experimental conditions including the electro-

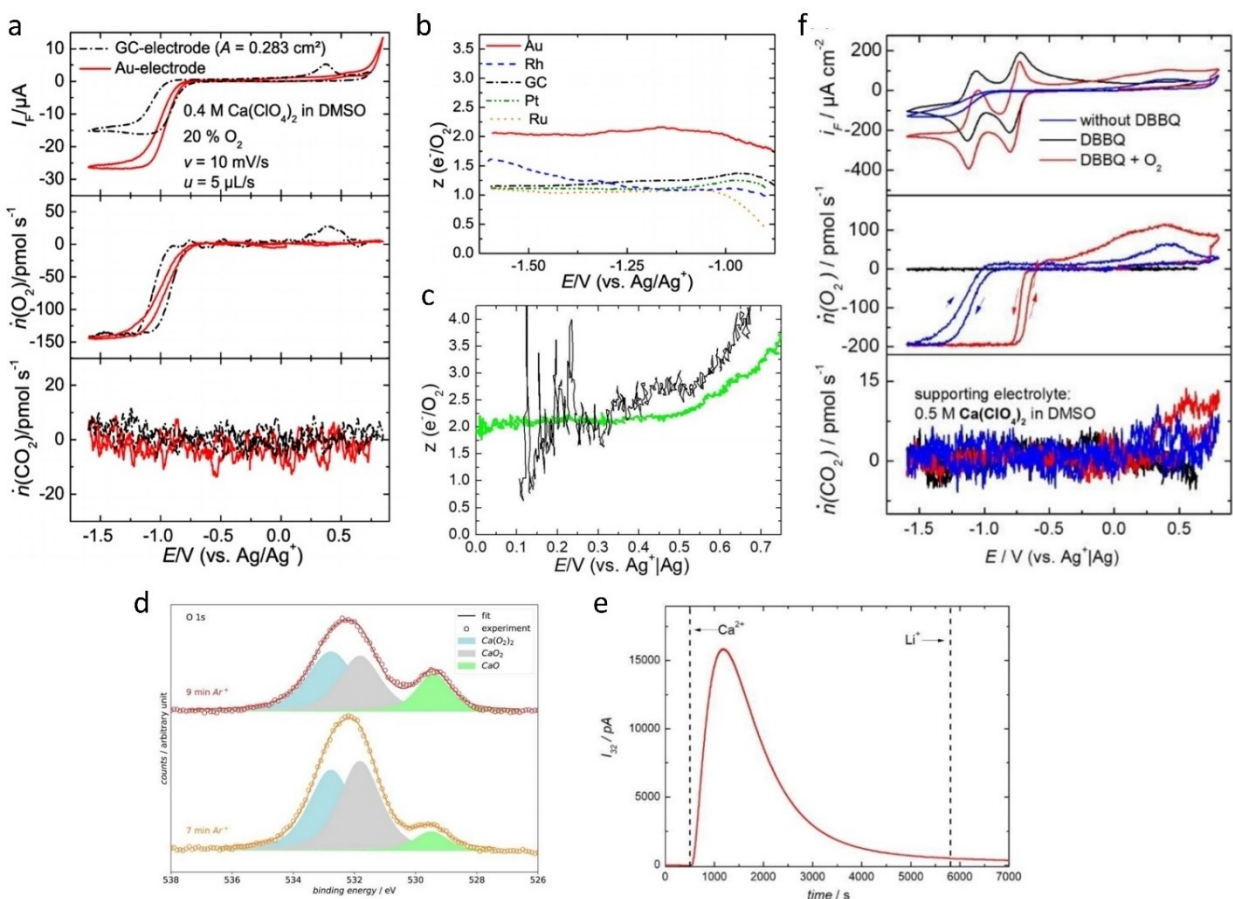
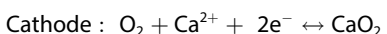
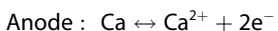


Figure 3. Mechanistic characterization of $\text{Ca}-\text{O}_2$ batteries. a) CV and OEMS results on GC and Au cathodes with $\text{Ca}(\text{ClO}_4)_2$ - DMSO electrolyte. The number of electrons transferred per oxygen molecule b) on multiple cathodes during reduction and c) on Au during oxidation. Reproduced from Ref. [29a] with permission. Copyright 2016, American Chemical Society. d) O 1s XPS spectra collected from the discharged Pt electrode after Ar^+ treatment. e) OEMS signal of the gas evolution from a stirred DMSO solution containing KO_2 after adding $\text{Ca}(\text{ClO}_4)_2$ and LiClO_4 . f) CV and OEMS data on an Au cathode in electrolytes containing DBBQ as a discharge mediator. Reproduced from Ref. [29b] with permission. Copyright 2020, The Authors.

lyte volume, electrode surface area, and actual discharge capacity. With a noticeable solubility of discharge product, the $\text{Ca}-\text{O}_2$ system based on $\text{Ca}(\text{O}_2)_2$ could behave like the $\text{K}-\text{O}_2$ system based on KO_2 , whose coulombic efficiency grows with cycling owing to the gradual saturation of KO_2 in the electrolyte.^[31]

The discharge product of the $\text{Ca}-\text{O}_2$ battery depends on the use of electrode materials. On the Au cathode, ORR proceeded at $\sim 2\text{e}^-/\text{O}_2$ from 2.6 V vs. Ca/Ca^{2+} (Figure 3, a and b), consistent with the formation of CaO_2 .^[29a]



The discharge products were also partly soluble.^[29] The discharge products were oxidized back to O_2 at $\sim 2\text{e}^-/\text{O}_2$ at low overpotentials but increased to $> 3\text{e}^-/\text{O}_2$ at high overpotentials (Figure 3c), probably due to side reactions that occurred during oxidation of the discharge product or by-products. XPS of the

discharged cathode indicates that the discharge products contained O species of various chemical states, including superoxide, peroxide and oxide (Figure 3d), along with S species (attributed to the decomposition of DMSO by Pt or ${}^1\text{O}_2$), and were covered by a carbon-rich passivating layer, which can be attributed to CO_3^{2-} salts resulting from side reactions involving superoxide and ${}^1\text{O}_2$.^[9,29b]

We notice that the ORR mechanism appears to depend on the concentration of Ca^{2+} . The above experiments were conducted with $0.1 \text{ M} \sim 0.4 \text{ M} \text{Ca}(\text{ClO}_4)_2$ in DMSO. When increasing the concentration of $\text{Ca}(\text{ClO}_4)_2$ to 1.0 M, mixing of the electrolyte with a KO_2 solution led to immediate O_2 evolution (Figure 3e). This indicates that O_2^- disproportionation can be catalyzed in the bulk solution by 1.0 M Ca^{2+} in addition to specific cathode materials such as Au.

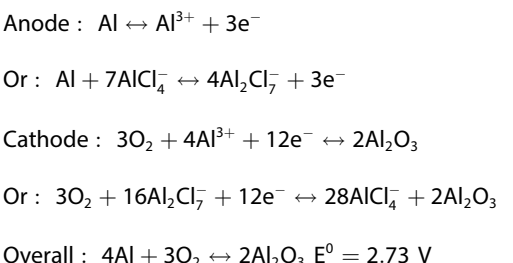
In the above chemical mixing experiment (Figure 3e), OER was observed together with the formation of CO , CO_2 , SO_2 , H_2O and CH_2O as detected by mass spectrometer,^[29b] which indicates that the disproportionation reaction is accompanied by the formation of ${}^1\text{O}_2$. ${}^1\text{O}_2$ was shown to originate from superoxide disproportionation and attack electrolyte to evolve parasitic gases.^[9c] This experiment provides insights into the

origin of the by-products found in the XPS results (Figure 3d). Future studies including detection of $^{1}\text{O}_2$ using fluoroscopy^[9b] or UV-Vis spectroscopy,^[9d] are needed to identify the underlying reactions.

Reinsberg *et al.* reported using 2,5-di-tert-butyl-1,4-benzoquinone (DBBQ) as a discharge mediator for Ca–O₂ batteries (Figure 3f).^[29b] The DBBQ mediator enhanced both ORR and OER currents. Both ORR and OER onset overpotentials were drastically decreased by ~0.25 V, resulting in almost zero overpotential. The authors suggested a mix of $1\text{e}^-/\text{O}_2$ and $2\text{e}^-/\text{O}_2$ processes in the DBBQ-mediated ORR based on RDE and OEMS data. Other material characterization techniques including XRD and XPS could be used to verify the final products of the system at various Ca²⁺ concentrations.

2.4. Al–O₂ Batteries

Aqueous Al–O₂ batteries are primary batteries due to the difficulty in plating Al metal ($E^0 = -1.66$ V vs. SHE) in aqueous electrolytes, where Al corrosion currents are high in the order of 10^1 to 10^2 mA/cm².^[32] Reversible Al plating and stripping with CE as high as 99.7%^[33] and corrosion rate as low as the 10^{-3} mA/cm² scale^[34] have been demonstrated in Al(TFSI)₃ in acetonitrile,^[35] ionic liquids^[36] and ionic liquids analogue.^[33,37] Plausible reactions of rechargeable Al–O₂ batteries in a simple-salt-based electrolyte or Lewis-acidic ionic liquid that contains chloroaluminate ion (Al_xCl_y⁻) could be as following:^[34]



To the best of our knowledge, the first rechargeable Al–O₂ battery was demonstrated in Lewis-acidic ionic liquids [AlCl₃ in 1-ethyl-3-methylimidazolium chloride (EMImCl)].^[34] Despite a theoretical $E^0 = 2.73$ V for Al₂O₃-based Al–O₂ batteries, the battery displayed low discharge voltages ranging from 0.5 V to 0.75 V at various current densities (Figure 4a). To enable separate measurement of the voltages of anode and cathode, a three-electrode cell was used with a tungsten (W) pseudo-reference electrode, which was calibrated to be 2.45 vs. Al/Al³⁺ (0 V vs. W = 2.45 V vs. Al/Al³⁺). The cathode showed an open circuit voltage (OCV), discharge potential, and charge potential at +0.43 V, -0.35 V and +1.4 V vs. W, respectively, translating to 2.88 V, 2.10 V and 3.85 V vs. Al/Al³⁺, respectively (Figure 4b). The OCV agrees well with the theoretical $E^0 = 2.73$ V for Al₂O₃-based Al–O₂ batteries. The low discharge cell voltage largely originates from the Al counter electrode, which showed OCV, oxidation voltage and reduction voltage of -0.93 V, -0.85 V and -1.0 V vs. W, translating to 1.52 V, 1.60 V and 1.45 V vs. Al/Al³⁺. This represents a substantial ~1.5 V systematic positive

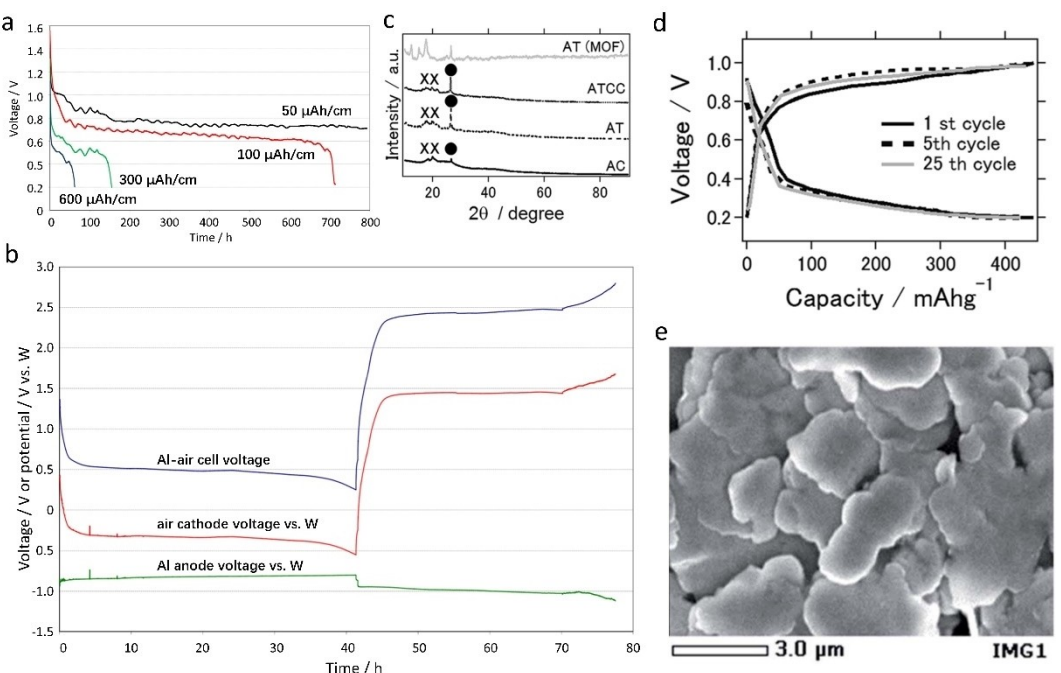


Figure 4. Mechanistic characterization of Al–O₂ batteries. a) Discharge curves of Al-air cells using EMIm/AlCl₃ electrolyte at different current densities. b) Discharge-charge curve at 600 $\mu\text{Ah}/\text{cm}^2$ of an Al-air battery equipped with a tungsten pseudo-reference. Reproduced from Ref. [34] with permission. Copyright 2014, Elsevier. c) XRD pattern of the discharged air cathode. Reproduced from Ref. [38] with permission. Published by The Royal Society of Chemistry. d) Discharge-charge curve at 500 $\mu\text{Ah}/\text{cm}^2$ of an Al-air battery with a TiC cathode. e) SEM image of the discharged TiC cathode. Reproduced from Ref. [39] under the terms of the Creative Commons License. Copyright 2017, The Authors.

shift in the Al electrode potential. We suggest that this shift could be associated with the formation of a passivation layer on the Al electrode, as revealed in a later work by XPS where the same electrolyte was used.^[38] The layer could be generated from reaction between fresh Al and O₂, yielding Al₂O₃ that could increase the Al anode potential from Al/AlCl₄⁻ to Al/Al₂O₃. Overall, these observations indicate that the Al–O₂ battery with an ionic liquid electrolyte display a cathode potential that is consistent with the formation of Al₂O₃, although accompanied by a high roundtrip cathode overpotential of 1.75 V. In addition, the drastically different potentials between the Al metal electrode in inert and oxidative environment highlights the importance of using three-electrode cells with a non-O₂-sensitive reference electrode in the study of multivalent metal–O₂ batteries.

Rechargeable Al–O₂ batteries are further studied using the same ionic liquids (EMImCl)^[38–40] and other ionic-liquid-analogues (AlCl₃ in acetamide and AlCl₃ in urea).^[41] Stable cycling profiles (Figure 4d) and film-like discharge product morphology (Figure 4e) were reported on a TiC cathode.^[39] XRD revealed the formation of Al₂O₃ and Al(OH)₃ phases (Figure 4c) on the cycled carbon cathode,^[38] which could be the product of ORR. Note that the above-mentioned electrolytes contain chloroaluminate ion (Al_xCl_y⁻), which reacts violently with water to yield HCl and white solid.^[42] Unfortunately, the above works were conducted using air or dry air, which could contain moisture to some extent and introduce Al₂O₃ or Al(OH)₃ into the discharge product.^[41] To realize practical use, new electrolyte systems that are not sensitive to air must be developed.

3. Experiences Learned from Li–O₂ Batteries

The development of Li–O₂ batteries demonstrates the importance of comprehensive mechanistic investigations. The discharge and charge products should be carefully investigated using quantitative techniques.

In the early stage of research on Li–O₂ batteries, carbonate solvents were widely used due to their successful application in Li-ion batteries. In the discharged cathodes, Li₂O₂ was found using Raman^[43] and XRD^[44] back in 1996. O₂ consumption during discharge was quantified by measuring water displacement to give e⁻/O₂ ratios between 2 and 4, which was attributed to a mixture of Li₂O₂ and Li₂O production.^[45] Gas evolution in charging a Li₂O₂-prefilled cathode characterized using OEMS revealed evolution of O₂ and CO₂, although the amounts were not quantified.^[44] These findings appear to suggest that the conversion between O₂ and Li₂O₂ is the main reaction in reported Li–O₂ batteries.

However, more characterizations later found a different conclusion.^[46] Comprehensive characterization using transmission electron microscopy (TEM), XRD, Fourier-transform infrared spectroscopy (FTIR), nuclear magnetic resonance (NMR), Raman [including surface-enhanced Raman spectroscopy (SERS)] and OEMS revealed that instead of Li₂O₂, lithium (alkyl)carbonates are the predominant discharge product in carbonate-based electrolytes.^[47] The underlying mechanism is that ORR begins

with the formation of the nucleophilic superoxide, which reacts with the carbonate solvent to generate lithium (alkyl) carbonates.^[47d,48] These by-products are also oxidizable leading to an apparently rechargeable cell, except that their oxidation yields CO₂ and other parasitic gas instead of O₂.^[47c]

To realize the intended reduction of O₂ to Li₂O₂, solvents that are stable against superoxide, e.g. DME and DMSO, should be used. Li₂O₂ formation in stable solvents is supported by XRD, Raman, FTIR and *in situ* XPS.^[47c,49] More importantly, O₂ and Li₂O₂ reactions are quantified. As a direct measurement of the degree of stability in discharge-charge cycle, O₂ consumption during discharge and evolution during charge were quantified by the use of pressure gauge and OEMS.^[47c,49b,50] In complementary, the amount of Li₂O₂ has also been quantified, using titration and TiOSO₄-based colorimetry.^[51] To probe the extent of instability, by-product formation during discharge and charge was characterized by FTIR, NMR and powder XRD (PXRD).^[49b] A method to quantify by-product by transforming them into CO₂ using Fenton's reagent followed by its quantification using OEMS was proposed.^[52] Together, these comprehensive investigations picture the reversible transformation between O₂ and Li₂O₂ via ORR and OER with high certainty.

Alternative to Li₂O₂, other stable discharge products have also been reported with advanced characterizations. Using a cathode based on reduced graphene oxide and Ir nanoparticles, LiO₂ is stabilized and precipitates as a crystalline product, as supported by SEM, TEM, high-energy XRD (HE-XRD), Raman, XPS, electron paramagnetic resonance (EPR) and FTIR.^[53] In a molten salt electrolyte catalyzed by a Ni catalyst, reversible Li₂O formation and decomposition is characterized using XRD, Raman, SEM, XPS and rotating ring-disc electrode (RDE).^[54]

Studies on the discharge mechanism are vital for understanding and controlling the discharge stability, rate capability and capacity. During discharge, lithium superoxide (including LiO₂ and the dissociated O₂⁻) were identified as the first intermediate from O₂ reduction with evidence from CV and *in situ* SERS.^[55] In stable solvents such as ethers, the fate of O₂⁻ is strongly influenced by the electrolyte environment.^[56] It remains as O₂⁻ in the presence of only large cations like tetrabutylammonium ion (TBA⁺), and disproportionate into O₂²⁻ and O₂ in the presence of small ones like Li⁺, which can be explained using the hard-soft-acid-base (HSAB) theory.^[30,55a] As an intermediate, LiO₂ displays minor solubility depending on the solvent in the electrolyte, which results in two reaction pathways as probed by RRDE. In the solution-pathway, LiO₂ dissolves into the electrolyte where it disproportionates subsequently. In the surface-pathway, LiO₂ is adsorbed on the cathode where it disproportionates or obtains a second e⁻ to yield Li₂O₂.^[10a,57] SEM showed that the competition between these two pathways, which highly depends on the property of solvents, plays an important role in determining the morphology of the discharge product and thus the capacity and rate.^[10a] This competition is also controllable by the selection of anion, additives and current density.^[10b–d]

The charging mechanism is also studied in order to address the high charging overpotential. *Operando* XRD character-

ization of Li_2O_2 evolution during discharge and charge revealed a two-stage charging feature.^[58] *In situ* TEM and SEM were applied to study the morphological changes of Li_2O_2 and identify active reaction sites, which is important for catalyst design.^[59] Unlike the discharge reaction in which the intermediate has been well confirmed as O_2^- , the charge reaction is less understood and the nature of intermediates remains a topic of debate. A wide variety of techniques including SERS, *operando* XRD, X-ray absorption near edge structure (XANES), *in situ* selected-area electron diffraction (SAED) and RRDE have been applied to probe potential intermediates, e.g. O_2^- and $\text{Li}_{2-x}\text{O}_2$.^[55b,58b,60] Upon Charging, soluble superoxide has been observed using thin-film RRDE,^[60a,61] which can disproportionate to form nanocrystalline Li_2O_2 and evolve O_2 . Using aberration-corrected environmental TEM under an oxygen environment,^[60b] LiO_2 has been observed as an intermediate phase during part of the charge of a solid-state Li–O₂ battery, which implies metastability of LiO_2 when stabilized by a catalyst such as RuO_2 ^[60b] or Ir.^[53] More focus should be devoted to revealing the charging mechanism to guide future efforts in reducing the high charging overpotential.

Since Li–O₂ batteries display limited cycle life, addressing the instability is one of the most critical steps in advancing this technology to a practical level. A major cause of instability has now been recognized as the formation of ${}^1\text{O}_2$, an excited type of O₂ gas that displays high reactivity with electrolytes and electrodes.^[9] It was found to originate from O₂[−] disproportionation,^[9c] and oxidation of O₂[−] and/or Li_2O_2 ,^[9a,b] using multiple quantification techniques including *operando* EPR spectrometry, *operando* UV/Vis spectrometry (fluorescence and absorption) and HPLC, with the help of ${}^1\text{O}_2$ traps, e.g. 2,2,6,6-tetramethyl-4-piperidone (4-oxo-TEMP) or 9,10-dimeth-

ylanthracene (DMA).^[9] Identification of ${}^1\text{O}_2$ as a major source of parasitic reaction allows rational development of strategies to address the severe instability to realize reversible Li–O₂ batteries including quenchers^[62] and redox mediators.^[9d,63]

4. Summary and Outlook

To date, ORR and OER in Li–O₂ batteries have been intensively characterized by many advanced characterization techniques, and new characterization methods are still continuously emerging. These powerful tools enable researchers to establish a better understanding of the Li–O₂ reactions. These understandings serve as theoretical bases and roadmaps in developing new materials for better performances. Compared with the well-established mechanistic studies on Li–O₂ batteries, fundamental studies in many rechargeable multivalent metal–O₂ batteries are still in their infancy. The lack of understanding in reaction and degradation mechanisms has hindered further improvement of the performance of these systems. By leveraging the experiences in mechanistic studies on Li–O₂ batteries in the past decade, the development of multivalent chemistries can be accelerated. In Figure 5 we have summarized the current status of mechanistic studies on rechargeable metal–O₂ batteries, in the framework of how the mechanistic open questions have been answered, with Li–O₂ battery as an example. Future efforts are needed to answer the following crucial open questions:

1. What are the discharge products in these multivalent metal–O₂ batteries? How are they dependent on the ORR conditions, e.g. cathode material, electrolyte composition, current density and O₂ pressure?

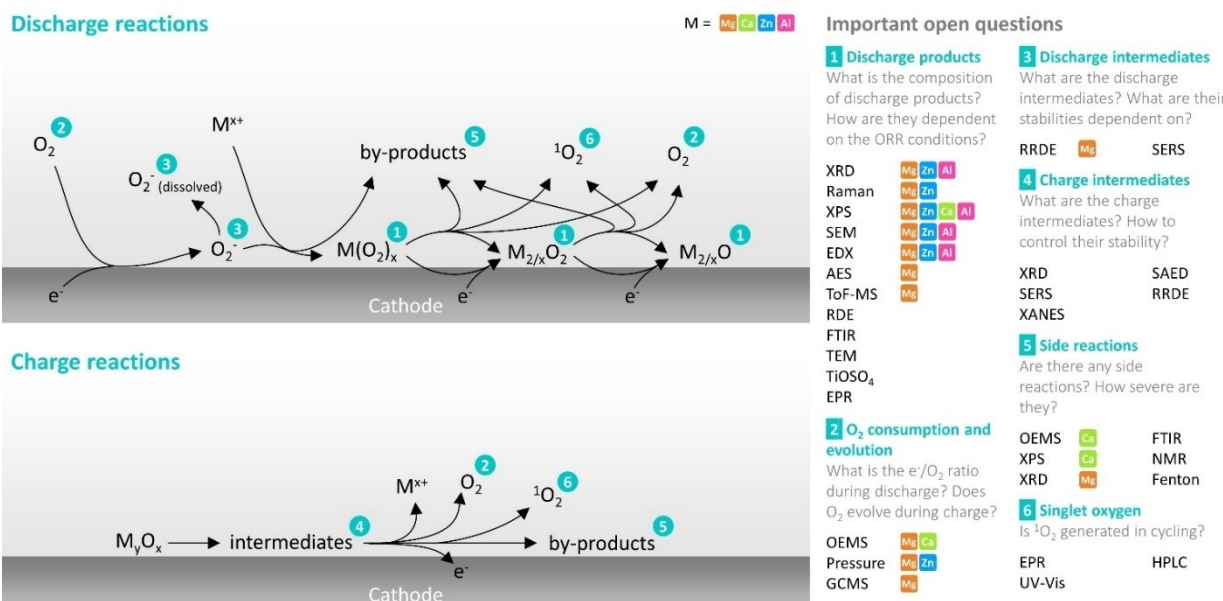


Figure 5. A summary of the important open questions and current status of mechanistic studies on rechargeable multivalent metal–O₂ batteries. The techniques that have been used to study mechanistic open questions in Li–O₂ batteries are listed. The symbols of multivalent elements next to each technique indicate that this technique has been applied to study the corresponding open question in the O₂ battery of those elements. Detailed discussions can be found in the corresponding sections.

2. Does O₂ evolve during charge? Do other parasitic gases evolve during charging? Are the O₂ consumption and evolution rates consistent with the discharge products?
3. What are the discharge intermediates? What is their stability dependent on? Multiple spectroscopic and electrochemical techniques could be applied in synergy to unambiguously identify the discharge intermediates. With these compositions identified, the effect of solvent, salt and additive on the stability and selectivity of these species can be investigated to maximum output capacity and power.
4. What are the charge intermediates? How to control their stability to reduce charge overpotential?
5. Are there any side reactions? How severe are they? The formation of by-products can be qualitatively and quantitatively analyzed to guide the development of stable electrolytes and electrodes.
6. What are the causes of the side reactions? ¹O₂ generation can be probed to help to understand the fate of missing O₂ in some chemistries, e.g. Mg—O₂ and Ca—O₂ batteries.

The development of rechargeable multivalent metal-O₂ batteries is critical in achieving batteries with high energy density, low cost, high safety and sustainability. The emergence of new metal-anode-friendly electrolytes has brought great opportunities to further studies on these less-understood chemistries. Guided by the critical insights generated from fundamental mechanistic studies, the full potential of rechargeable multivalent metal-O₂ batteries will be realized.

Acknowledgements

The work described in this work was supported by a grant from Research Grants Council (RGC) of the Hong Kong Special Administrative Region under CUHK14307919.

Conflict of Interest

The authors declare no conflict of interest.

Keywords: metal-oxygen batteries • oxygen electrodes • electrolytes • reaction mechanism • multivalent batteries

- [1] W. J. Kwak, Rosy, D. Sharon, C. Xia, H. Kim, L. R. Johnson, P. G. Bruce, L. F. Nazar, Y. K. Sun, A. A. Frimer, M. Noked, S. A. Freunberger, D. Aurbach, *Chem. Rev.* **2020**, *120*, 6626–6683.
- [2] W. Sun, F. Wang, B. Zhang, M. Zhang, V. Küpers, X. Ji, C. Theile, P. Bicker, K. Xu, C. Wang, *Science* **2021**, *371*, 46–51.
- [3] a) C. Y. Chen, K. Matsumoto, K. Kubota, R. Hagiwara, Q. Xu, *Adv. Energy Mater.* **2019**, *9*, 1900196; b) L. Ma, M. A. Schroeder, O. Borodin, T. P. Pollard, M. S. Ding, C. Wang, K. Xu, *Nat. Energy* **2020**, *5*, 743–749.
- [4] Y. Li, H. Dai, *Chem. Soc. Rev.* **2014**, *43*, 5257–5275.
- [5] a) F. Wang, O. Borodin, T. Gao, X. Fan, W. Sun, F. Han, A. Faraone, J. A. Dura, K. Xu, C. Wang, *Nat. Mater.* **2018**, *17*, 543–549; b) J. Zhang, J. Zhao, H. Du, Z. Zhang, S. Wang, G. Cui, *Electrochim. Acta* **2018**, *280*, 108–113; c) J. Zhao, J. Zhang, W. Yang, B. Chen, Z. Zhao, H. Qiu, S. Dong, X. Zhou, G. Cui, L. Chen, *Nano Energy* **2019**, *57*, 625–634; d) C. Zhang, J. Holoubek, X. Wu, A. Daniyar, L. Zhu, C. Chen, D. P. Leonard,

- I. A. Rodriguez-Perez, J. X. Jiang, C. Fang, X. Ji, *Chem. Commun.* **2018**, *54*, 14097–14099.
- [6] a) N. Zhang, F. Cheng, Y. Liu, Q. Zhao, K. Lei, C. Chen, X. Liu, J. Chen, *J. Am. Chem. Soc.* **2016**, *138*, 12894–12901; b) L. Wang, Y. Zhang, H. Hu, H. Y. Shi, Y. Song, D. Guo, X. X. Liu, X. Sun, *ACS Appl. Mater. Interfaces* **2019**, *11*, 42000–42005; c) Z. Zhao, J. Zhao, Z. Hu, J. Li, J. Li, Y. Zhang, C. Wang, G. Cui, *Energy Environ. Sci.* **2019**, *12*, 1938–1949; d) J. Huang, X. Chi, Q. Han, Y. Liu, Y. Du, J. Yang, Y. Liu, *J. Electrochem. Soc.* **2019**, *166*, A1211–A1216; e) H. Glatz, E. Tervoort, D. Kundu, *ACS Appl. Mater. Interfaces* **2020**, *12*, 3522–3530.
- [7] a) S. D. Han, N. N. Rajput, X. Qu, B. Pan, M. He, M. S. Ferrandon, C. Liao, K. A. Persson, A. K. Burrell, *ACS Appl. Mater. Interfaces* **2016**, *8*, 3021–3031; b) A. Naveed, H. Yang, J. Yang, Y. Nuli, J. Wang, *Angew. Chem. Int. Ed.* **2019**, *58*, 2760–2764; *Angew. Chem.* **2019**, *131*, 2786–2790; c) A. Naveed, H. Yang, Y. Shao, J. Yang, N. Yanna, J. Liu, S. Shi, L. Zhang, A. Ye, B. He, J. Wang, *Adv. Mater.* **2019**, *31*, e1900668; d) N. Zhang, Y. Dong, Y. Wang, Y. Wang, J. Li, J. Xu, Y. Liu, L. Jiao, F. Cheng, *ACS Appl. Mater. Interfaces* **2019**, *11*, 32978–32986.
- [8] H. Pan, Y. Shao, P. Yan, Y. Cheng, K. S. Han, Z. Nie, C. Wang, J. Yang, X. Li, P. Bhattacharya, K. T. Mueller, J. Liu, *Nat. Energy* **2016**, *1*, 16039.
- [9] a) J. Wandt, P. Jakes, J. Granwehr, H. A. Gasteiger, R. A. Eichel, *Angew. Chem. Int. Ed.* **2016**, *128*, 7006–7009; b) N. Mahne, B. Schafzahl, C. Leypold, M. Leypold, S. Grumm, A. Leitgeb, G. A. Strohmeier, M. Wilkening, O. Fontaine, D. Kramer, C. Slugovc, S. M. Borisov, S. A. Freunberger, *Nat. Energy* **2017**, *2*, 17036; c) E. Mourad, Y. K. Petit, R. Spezia, A. Samoilov, F. F. Summa, C. Prehal, C. Leypold, N. Mahne, C. Slugovc, O. Fontaine, S. Brutt, S. A. Freunberger, *Energy Environ. Sci.* **2019**, *12*, 2559–2568; d) Z. Liang, Q. Zou, J. Xie, Y.-C. Lu, *Energy Environ. Sci.* **2020**, *13*, 2870–2877.
- [10] a) L. Johnson, C. Li, Z. Liu, Y. Chen, S. A. Freunberger, P. C. Ashok, B. B. Praveen, K. Dholakia, J. M. Tarascon, P. G. Bruce, *Nat. Chem.* **2014**, *6*, 1091–1099; b) C. M. Burke, V. Pande, A. Khetan, V. Viswanathan, B. D. McCloskey, *PNAS* **2015**, *112*, 9293–9298; c) N. B. Aetukuri, B. D. McCloskey, J. M. Garcia, L. E. Krupp, V. Viswanathan, A. C. Luntz, *Nat. Chem.* **2015**, *7*, 50–56; d) B. D. Adams, C. Radtke, R. Black, M. L. Trudeau, K. Zaghib, L. F. Nazar, *Energy Environ. Sci.* **2013**, *6*, 1772.
- [11] N. B. Aetukuri, G. O. Jones, L. E. Thompson, C. Ozgit-Akgun, E. Akca, G. Demirci, H.-C. Kim, D. S. Bethune, K. Virwani, G. M. Wallraff, *ACS Energy Lett.* **2018**, *3*, 2342–2348.
- [12] B. Xie, H. S. Lee, H. Li, X. Q. Yang, J. McBreen, L. Q. Chen, *Electrochim. Commun.* **2008**, *10*, 1195–1197.
- [13] T. Song, O. Morales-Collazo, J. F. Brennecke, *Journal of Chemical & Engineering Data* **2019**, *64*, 4956–4967.
- [14] M. Balaish, A. Kraysberg, Y. Ein-Eli, *ChemElectroChem* **2014**, *1*, 90–94.
- [15] T. Zhang, Z. Tao, J. Chen, *Mater. Horiz.* **2014**, *1*, 196–206.
- [16] a) S. B. Son, T. Gao, S. P. Harvey, K. X. Steirer, A. Stokes, A. Norman, C. Wang, A. Cresce, K. Xu, C. Ban, *Nat. Chem.* **2018**, *10*, 532–539; b) S. Y. Ha, Y. W. Lee, S. W. Woo, B. Koo, J. S. Kim, J. Cho, K. T. Lee, N. S. Choi, *ACS Appl. Mater. Interfaces* **2014**, *6*, 4063–4073.
- [17] a) O. Mizrahi, N. Amir, E. Pollak, O. Chusid, V. Marks, H. Gottlieb, L. Larush, E. Zinigrad, D. Aurbach, *J. Electrochem. Soc.* **2007**, *155*, A103; b) H. S. Kim, T. S. Arthur, G. D. Allred, J. Zajicek, J. G. Newman, A. E. Rodnyansky, A. G. Oliver, W. C. Boggess, J. Muldoon, *Nat. Commun.* **2011**, *2*, 427; c) I. Shterenberg, M. Salama, H. D. Yoo, Y. Gofer, J.-B. Park, Y.-K. Sun, D. Aurbach, *J. Electrochim. Soc.* **2015**, *162*, A7118–A7128; d) R. E. Doe, R. Han, J. Hwang, A. J. Gmitter, I. Shterenberg, H. D. Yoo, N. Pour, D. Aurbach, *Chem. Commun.* **2014**, *50*, 243–245.
- [18] a) T. J. Carter, R. Mohtadi, T. S. Arthur, F. Mizuno, R. Zhang, S. Shirai, J. W. Kampf, *Angew. Chem. Int. Ed.* **2014**, *53*, 3173–3177; *Angew. Chem.* **2014**, *126*, 3237–3241; b) Y.-s. Guo, F. Zhang, J. Yang, F.-f. Wang, Y. Nu Li, S.-i. Hirano, *Energy Environ. Sci.* **2012**, *5*, 9100.
- [19] a) G. Vardar, E. G. Nelson, J. G. Smith, J. Naruse, H. Hiramatsu, B. M. Bartlett, A. E. S. Sleightholme, D. J. Siegel, C. W. Monroe, *Chem. Mater.* **2015**, *27*, 7564–7568; b) J. G. Smith, J. Naruse, H. Hiramatsu, D. J. Siegel, *Chem. Mater.* **2016**, *28*, 1390–1401.
- [20] P. Reinsberg, C. Bondu, H. Baltruschat, *Electrochim. Acta* **2016**, *200*, 214–221.
- [21] P. Fischer, P. Reinsberg, R. M. Schwarz, M. Marinaro, M. Wachtler, T. Diemant, R. J. Behm, H. Baltruschat, L. Jörissen, *J. Electrochim. Soc.* **2018**, *165*, A2037–A2046.
- [22] Q. Dong, X. Yao, J. Luo, X. Zhang, H. Hwang, D. Wang, *Chem. Commun.* **2016**, *52*, 13753–13756.
- [23] T. Shiga, Y. Hase, Y. Yagi, N. Takahashi, K. Takechi, *J. Phys. Chem. Lett.* **2014**, *5*, 1648–1652.

- [24] G. Vardar, J. G. Smith, T. Thompson, K. Inagaki, J. Naruse, H. Hiramatsu, A. E. S. Sleightholme, J. Sakamoto, D. J. Siegel, C. W. Monroe, *Chem. Mater.* **2016**, *28*, 7629–7637.
- [25] T. Shiga, Y. Hase, Y. Kato, M. Inoue, K. Takechi, *Chem. Commun.* **2013**, *49*, 9152–9154.
- [26] H. Tian, T. Gao, X. Li, X. Wang, C. Luo, X. Fan, C. Yang, L. Suo, Z. Ma, W. Han, C. Wang, *Nat. Commun.* **2017**, *8*, 14083.
- [27] B. J. Bergner, A. Schurmann, K. Peppler, A. Garsuch, J. Janek, *J. Am. Chem. Soc.* **2014**, *136*, 15054–15064.
- [28] a) P. Ponrouch, C. Frontera, F. Barde, M. R. Palacin, *Nat. Mater.* **2016**, *15*, 169–172; b) D. Wang, X. Gao, Y. Chen, L. Jin, C. Kuss, P. G. Bruce, *Nat. Mater.* **2018**, *17*, 16–20; c) A. Shyamsunder, L. E. Blanc, A. Assoud, L. F. Nazar, *ACS Energy Lett.* **2019**, *4*, 2271–2276.
- [29] a) P. Reinsberg, C. J. Bondue, H. Baltruschat, *J. Phys. Chem. C* **2016**, *120*, 22179–22185; b) P. P. Bawol, P. H. Reinsberg, A. Koellisch-Mirbach, C. J. Bondue, H. Baltruschat, *ChemSusChem* **2020**, *14*, 428–400.
- [30] C. J. Allen, J. Hwang, R. Kautz, S. Mukerjee, E. J. Plichta, M. A. Hendrickson, K. M. Abraham, *J. Phys. Chem. C* **2012**, *116*, 20755–20764.
- [31] W. Wang, N. C. Lai, Z. Liang, Y. Wang, Y. C. Lu, *Angew. Chem. Int. Ed.* **2018**, *57*, 5042–5046; *Angew. Chem.* **2018**, *130*, 5136–5140.
- [32] J. Ryu, M. Park, J. Cho, *Adv. Mater.* **2019**, *31*, e1804784.
- [33] M. Angell, C.-J. Pan, Y. Rong, C. Yuan, M.-C. Lin, B.-J. Hwang, H. Dai, *PNAS* **2017**, *114*, 834–839.
- [34] R. Revel, T. Audichon, S. Gonzalez, *J. Power Sources* **2014**, *272*, 415–421.
- [35] M. Chiku, S. Matsumura, H. Takeda, E. Higuchi, H. Inoue, *J. Electrochem. Soc.* **2017**, *164*, A1841–A1844.
- [36] a) Y. Zhao, T. J. Van der Noot, *Electrochim. Acta* **1997**, *42*, 1639–1643; b) T. Jiang, M. J. Chollier Brym, G. Dubé, A. Lasia, G. M. Brisard, *Surf. Coat. Technol.* **2006**, *201*, 1–9; c) T. Jiang, M. J. Chollier Brym, G. Dubé, A. Lasia, G. M. Brisard, *Surf. Coat. Technol.* **2006**, *201*, 10–18; d) S. Zein El Abedin, E. M. Moustafa, R. Hempelmann, H. Natter, F. Endres, *ChemPhysChem* **2006**, *7*, 1535–1543.
- [37] H. M. Abood, A. P. Abbott, A. D. Ballantyne, K. S. Ryder, *Chem. Commun.* **2011**, *47*, 3523–3525.
- [38] R. Mori, *RSC Adv.* **2017**, *7*, 6389–6395.
- [39] R. Mori, *Sustain. Energy Fuels* **2017**, *1*, 1082–1089.
- [40] N. Bogolowski, J.-F. J. E. T. Drillet, *ECS Trans.* **2017**, *75*, 85.
- [41] N. Bogolowski, J.-F. Drillet, *Electrochim. Acta* **2018**, *274*, 353–358.
- [42] a) T. Tsuda, R. Hagiwara, *J. Fluorine Chem.* **2008**, *129*, 4–13; b) D. Gelman, B. Shvartsev, Y. Ein-Eli, *J. Mater. Chem. A* **2014**, *2*, 20237–20242.
- [43] a) K. M. Abraham, Z. Jiang, *J. Electrochem. Soc.* **1996**, *143*, 1–5; b) A. Debart, A. J. Paterson, J. Bao, P. G. Bruce, *Angew. Chem. Int. Ed.* **2008**, *47*, 4521–4524; *Angew. Chem.* **2008**, *120*, 4597–4600.
- [44] T. Ogasawara, A. Débart, M. Holzapfel, P. Novák, P. G. Bruce, *J. Am. Chem. Soc.* **2006**, *128*, 1390–1393.
- [45] J. Read, *J. Electrochem. Soc.* **2002**, *149*, A1190.
- [46] a) S. A. Freunberger, Z. Peng, L. J. Hardwick, Y. Chen, F. Barde, P. Bruce, in *Proceedings of the 218th Electrochemical Society Meeting, Las Vegas, NV, 2010*; b) K. Takechi, E. Sudo, T. Inaba, F. Mizuno, H. Nishikoori, T. Shiga, in *218th ECS Meeting, Las Vegas, NV, October 10–15, 2010*.
- [47] a) F. Mizuno, S. Nakanishi, Y. Kotani, S. Yokoishi, H. Iba, *Electrochemistry* **2010**, *78*, 403–405; b) W. Xu, V. V. Viswanathan, D. Wang, S. A. Towne, J. Xiao, Z. Nie, D. Hu, J.-G. Zhang, *J. Power Sources* **2011**, *196*, 3894–3899; c) B. D. McCloskey, D. S. Bethune, R. M. Shelby, G. Girishkumar, A. C. Luntz, *J. Phys. Chem. Lett.* **2011**, *2*, 1161–1166; d) S. A. Freunberger, Y. Chen, Z. Peng, J. M. Griffin, L. J. Hardwick, F. Barde, P. Novák, P. G. Bruce, *J. Am. Chem. Soc.* **2011**, *133*, 8040–8047.
- [48] V. S. Bryantsev, M. Blanco, *J. Phys. Chem. Lett.* **2011**, *2*, 379–383.
- [49] a) C. O. Laoire, S. Mukerjee, E. J. Plichta, M. A. Hendrickson, K. M. Abraham, *J. Electrochem. Soc.* **2011**, *158*, A302; b) Y. Chen, S. A. Freunberger, Z. Peng, F. Barde, P. G. Bruce, *J. Am. Chem. Soc.* **2012**, *134*, 7952–7957; c) S. A. Freunberger, Y. Chen, N. E. Drewett, L. J. Hardwick, F. Barde, P. G. Bruce, *Angew. Chem. Int. Ed.* **2011**, *50*, 8609–8613; *Angew. Chem.* **2011**, *123*, 8768–8772; d) Y. C. Lu, E. J. Crumlin, G. M. Veith, J. R. Harding, E. Mutoro, L. Baggetto, N. J. Dudney, Z. Liu, Y. Shao-Horn, *Sci. Rep.* **2012**, *2*, 715.
- [50] B. D. McCloskey, D. S. Bethune, R. M. Shelby, T. Mori, R. Scheffler, A. Speidel, M. Sherwood, A. C. Luntz, *J. Phys. Chem. Lett.* **2012**, *3*, 3043–3047.
- [51] a) B. D. McCloskey, A. Valery, A. C. Luntz, S. R. Gowda, G. M. Wallraff, J. M. Garcia, T. Mori, L. E. Krupp, *J. Phys. Chem. Lett.* **2013**, *4*, 2989–2993; b) P. Hartmann, C. L. Bender, J. Sann, A. K. Durr, M. Jansen, J. Janek, P. Adelhelm, *Phys. Chem. Chem. Phys.* **2013**, *15*, 11661–11672; c) K. U. Schwenke, M. Metzger, T. Restle, M. Piana, H. A. Gasteiger, *J. Electrochem. Soc.* **2015**, *162*, A573–A584.
- [52] M. M. Ottakam Thotiyil, S. A. Freunberger, Z. Peng, P. G. Bruce, *J. Am. Chem. Soc.* **2013**, *135*, 494–500.
- [53] J. Lu, Y. J. Lee, X. Luo, K. C. Lau, M. Asadi, H. H. Wang, S. Brombosz, J. Wen, D. Zhai, Z. Chen, D. J. Miller, Y. S. Jeong, J. B. Park, Z. Z. Fang, B. Kumar, A. Salehi-Khojin, Y. K. Sun, L. A. Curtiss, K. Amine, *Nature* **2016**, *529*, 377–382.
- [54] C. Xia, C. Kwok, L. Nazar, *Science* **2018**, *361*, 777–781.
- [55] a) C. O. Laoire, S. Mukerjee, K. Abraham, E. J. Plichta, M. A. Hendrickson, *J. Phys. Chem. C* **2009**, *113*, 20127–20134; b) Z. Peng, S. A. Freunberger, L. J. Hardwick, Y. Chen, V. Giordani, F. Barde, P. Novák, D. Graham, J. M. Tarascon, P. G. Bruce, *Angew. Chem. Int. Ed.* **2011**, *50*, 6351–6355; *Angew. Chem.* **2011**, *123*, 6475–6479.
- [56] B. Genorio, J. Staszak-Jirkovský, R. S. Assary, J. G. Connell, D. Strmcnik, C. E. Diesendruck, P. P. Lopes, V. R. Stamenkovic, J. S. Moore, L. A. Curtiss, *J. Phys. Chem. C* **2016**, *120*, 15909–15914.
- [57] C. O. Laoire, S. Mukerjee, K. Abraham, E. J. Plichta, M. A. Hendrickson, *J. Phys. Chem. C* **2010**, *114*, 9178–9186.
- [58] a) H. Lim, E. Yilmaz, H. R. Byon, *J. Phys. Chem. Lett.* **2012**, *3*, 3210–3215; b) S. Ganapathy, B. D. Adams, G. Stenou, M. S. Anastasaki, K. Goubitz, X. F. Miao, L. F. Nazar, M. Wagemaker, *J. Am. Chem. Soc.* **2014**, *136*, 16335–16344.
- [59] a) R. Wen, M. Hong, H. R. Byon, *J. Am. Chem. Soc.* **2013**, *135*, 10870–10876; b) L. Zhong, R. R. Mitchell, Y. Liu, B. M. Gallant, C. V. Thompson, J. Y. Huang, S. X. Mao, Y. Shao-Horn, *Nano Lett.* **2013**, *13*, 2209–2214; c) H. Zheng, D. Xiao, X. Li, Y. Liu, Y. Wu, J. Wang, K. Jiang, C. Chen, L. Gu, X. Wei, Y. S. Hu, Q. Chen, H. Li, *Nano Lett.* **2014**, *14*, 4245–4249; d) A. Kushima, T. Koido, Y. Fujiwara, N. Kuriyama, N. Kusumi, J. Li, *Nano Lett.* **2015**, *15*, 8260–8265.
- [60] a) Y. Wang, N.-C. Lai, Y.-R. Lu, Y. Zhou, C.-L. Dong, Y.-C. Lu, *Joule* **2018**, *2*, 2364–2380; b) L. Luo, B. Liu, S. Song, W. Xu, J. G. Zhang, C. Wang, *Nat. Nanotechnol.* **2017**, *12*, 535–539.
- [61] Y. Wang, Z. Liang, Q. Zou, G. Cong, Y.-C. Lu, *J. Phys. Chem. C* **2016**, *120*, 6459–6466.
- [62] Y. K. Petit, C. Leypold, N. Mahne, E. Mourad, L. Schafzahl, C. Slugovc, S. M. Borisov, S. A. Freunberger, *Angew. Chem. Int. Ed.* **2019**, *58*, 6535–6539; *Angew. Chem.* **2019**, *131*, 6605–6609.
- [63] W.-J. Kwak, S. A. Freunberger, H. Kim, J. Park, T. T. Nguyen, H.-G. Jung, H. R. Byon, Y.-K. Sun, *ACS Catal.* **2019**, *9*, 9914–9922.

Manuscript received: January 30, 2021

Revised manuscript received: March 18, 2021

Accepted manuscript online: March 18, 2021

Version of record online: March 30, 2021